

2-9-2010

SPINS : spectral phase interrogation using nonlinear spectra

Brook Jilek

Follow this and additional works at: https://digitalrepository.unm.edu/ose_etds

Recommended Citation

Jilek, Brook. "SPINS : spectral phase interrogation using nonlinear spectra." (2010). https://digitalrepository.unm.edu/ose_etds/10

This Thesis is brought to you for free and open access by the Engineering ETDs at UNM Digital Repository. It has been accepted for inclusion in Optical Science and Engineering ETDs by an authorized administrator of UNM Digital Repository. For more information, please contact disc@unm.edu.

Brook Anton Jilek

Candidate

Optical Science and Engineering

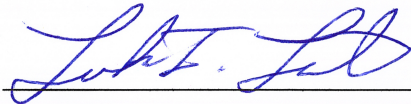
Department

This **thesis** is approved, and it is acceptable in quality and form for publication on microfilm:

Approved by the Thesis Committee:



, Chairperson



Accepted:

Dean, Graduate School

Date

SPINS: Spectral Phase Interrogation using Nonlinear Spectra

by

Brook Anton Jilek

B.S., Mathematics, New Mexico Institute of Mining and Technology,
2003

B.S., Physics with option in Atmospheric Physics, New Mexico
Institute of Mining and Technology, 2003

THESIS

Submitted in Partial Fulfillment of the
Requirements for the Degree of

Master of Science
Optical Science and Engineering

The University of New Mexico

Albuquerque, New Mexico

December, 2009

©2009, Brook Anton Jilek

Dedication

To my wife Evie.

And God hath given to me to speak as I would, and to conceive thoughts worthy of those things that are given me: because he is the guide of wisdom, and the director of the wise. For in his hand are both we, and our words, and all wisdom, and the knowledge and skill of works. For he hath given me the true knowledge of the things that are: to know the disposition of the whole world, and the virtues of the elements, the beginning, and ending, and midst of the times, the alterations of their courses, and the changes of seasons, the revolutions of the year, and the dispositions of the stars, the natures of living creatures, and rage of wild beasts, the force of winds, and reasonings of men, the diversities of plants, and the virtues of roots. And all such things as are hid, and not foreseen, I have learned: for wisdom, which is the worker of all things, taught me.

Wisdom 7:15-21

Acknowledgements

I would like to thank my advisor, Dr. Mansoor Sheik-Bahae, for presenting me with this very interesting thesis topic. I very much appreciate his *joie de vivre* and his dedication to keeping physics fun. I also am greatly indebted to him for teaching me most of what I know about lasers and nonlinear optics.

I would also like to thank all the other professors at UNM who have taught classes I've taken over the past few years. I have found you all to possess high moral character and astute minds. Thank you for making my graduate experience at UNM a good one.

I am grateful for the support of my boss, Dr. Donald Voss, supervisor, Alex Lovesee, and program manager, Dr. Tom Nelson for the opportunity to use the resources at Sandia National Labs to obtain and analyze the data presented in this thesis. My coworker, Ian Kohl, aligned and optimized the OPCPA laser used in obtaining the data. Without his help, there would be no data. I also owe a debt of gratitude to Drs. Erik Zeek and Daniel Bender, who have both helped tremendously in the development of the retrieval algorithm. They have saved me from many programming pitfalls. Thank you for having mercy on a poor programmer. Thanks also to Dave Catanach who helped me a lot with the typesetting.

And last, but not least, thanks to my beautiful wife, Evie, who has (mostly) patiently endured six years of grad school for this end.

Acknowledgements

SPINS: Spectral Phase Interrogation using Nonlinear Spectra

by

Brook Anton Jilek

ABSTRACT OF THESIS

Submitted in Partial Fulfillment of the
Requirements for the Degree of

Master of Science
Optical Science and Engineering

The University of New Mexico

Albuquerque, New Mexico

December, 2009

SPINS: Spectral Phase Interrogation using Nonlinear Spectra

by

Brook Anton Jilek

B.S., Mathematics, New Mexico Institute of Mining and Technology,
2003

B.S., Physics with option in Atmospheric Physics, New Mexico
Institute of Mining and Technology, 2003

M.S., Optical Science and Engineering, University of New Mexico,
2009

Abstract

A novel technique for ultrafast pulse measurement is presented. This technique involves only the measurement of the fundamental, second harmonic, and third harmonic (or other third-order nonlinear) spectra of an ultrafast pulse. An algorithm is employed to generate trial SHG and THG spectra based on the measured fundamental spectrum and a trial phase. The phase is adjusted iteratively until the best match between the trial and measured SHG and THG spectra is obtained. The technique is experimentally simple, not subject to delicate temporal alignments, and potentially insensitive to wavefront quality.

Contents

Acknowledgements	v
List of Figures	xi
1 Introduction	1
1.1 Definitions	1
1.2 History of the measurement problem	2
1.3 Fringe-Resolved Autocorrelation (FRAC)	4
1.4 Frequency-Resolved Optical Gating (FROG)	8
1.5 Spectral Phase Interferometry for Direct Electric field Reconstruction (SPIDER)	11
1.6 SPINS	14
2 Algorithm Development	17
2.1 Uniqueness of solution	17
2.2 Sensitivity to phase	20

CONTENTS

2.3	Resiliency to noise	24
3	Experimental Validation	32
3.1	Purpose	32
3.2	Experimental Setup	32
3.3	Procedure	34
3.4	Results	34
4	Conclusion	42
5	Future Work	44
	References	46

List of Figures

1.1	Experimental setup for intensity autocorrelation	3
1.2	Experimental setup for interferometric autocorrelation	5
1.3	Examples of fringe-resolved autocorrelation traces. Top row: a 10 fs Gaussian intensity. Second row: a 7 fs <i>sech</i> ² intensity. Third row: a pulse with considerable TOD. Fourth row: a double pulse.	6
1.4	Examples of MOSAIC traces compared to FRAC traces. Chirp is varied in each case by making the pulses travel through a 6-mm-thick <i>SiO</i> ₂ window for (a) zero, (b) two, (c) three, and (d) five passes. . .	8
1.5	Setup for single-shot SHG FROG.	9
1.6	Experimental setup for SPIDER.	12
1.7	Flow chart describing the SPIDER algorithm.	13
2.1	Pulse in time domain with GVD = 50,000 <i>fs</i> ² and TOD = -10,000,000 <i>fs</i> ³ compared to transform-limited pulse.	18

LIST OF FIGURES

2.2	Error map for pulse with known GVD = $50,000 fs^2$ and TOD = $-10,000,000 fs^3$. The log of the error is plotted. Solutions are at blue points.	19
2.3	3D Error map for pulse with known GVD = $50,000 fs^2$ and TOD = $-10,000,000 fs^3$. Note the two points where the error is exceedingly small. These are the two solutions.	20
2.4	Pulse in time domain with GVD = $50,000 fs^2$, TOD = $-10^7 fs^3$, and FOD = $-10^8 fs^4$ compared to transform-limited pulse.	21
2.5	Plot showing the differences in SHG spectra between a transform-limited pulse and one with phase that causes a 43% stretching in time domain	22
2.6	Plot showing the differences in THG spectra between a transform-limited pulse and one with phase that causes a 43% stretching in time domain	22
2.7	Transform-limited FROG image	23
2.8	FROG image of pulse with non-zero phase	23
2.9	Difference between the transform-limited and non-zero phase FROG images	24
2.10	Phase retrieval using simplex method with 0.8% noise. Known phase (dark blue) and retrieved phase (green) are almost indistinguishable.	26
2.11	Retrieved (orange) and computed (green) SHG spectra with 0.8% noise.	27
2.12	Retrieved (orange) and computed (green) THG spectra with 0.8% noise.	27

LIST OF FIGURES

2.13	Phase retrieval using simplex method with 1 percent noise. Known phase (dark blue) and conjugate of the retrieved phase (red) deviate noticeably in the pulse wings.	28
2.14	Retrieved (orange) and computed (green) SHG spectra with 1 percent noise.	29
2.15	Retrieved (orange) and computed (green) THG spectra with 1 percent noise.	29
2.16	Phase retrieval using simplex method with 1.1% noise. Known phase (dark blue, hardly visible) and conjugate of the retrieved phase (red) are almost identical.	30
2.17	Retrieved (orange) and computed (green) SHG spectra with 1.1% noise.	31
2.18	Retrieved (orange) and computed (green) THG spectra with 1.1% noise.	31
3.1	Experimental setup for SPINS.	33
3.2	Fundamental spectra as recorded for 4 different shots	35
3.3	SHG spectra as recorded for 4 different shots with different GVD.	35
3.4	THG spectra as recorded for 4 different shots with different GVD.	36
3.5	Fundamental spectra as recorded by the imaging spectrometer (green) and retrieved by FROG (blue).	37
3.6	Fundamental, SHG, and THG spectra used as input to SPINS algorithm.	38
3.7	Measured FROG image. Wavelength is on the horizontal axis and delay is on the vertical axis.	38

LIST OF FIGURES

3.8	Comparison of SPINS and FROG phase retrievals. SPINS-retrieved phase (red) differs markedly from FROG-retrieved phase (dark blue).	39
3.9	Comparison of SHG spectra: SPINS-retrieved (blue), FROG-retrieved (green) and measured (red).	40
3.10	Comparison of THG spectra: SPINS-retrieved (blue), FROG-retrieved (green) and measured (red).	40

Chapter 1

Introduction

1.1 Definitions

The electric field of a pulse is defined in the frequency domain as a spectral amplitude times a spectral phase. If the measured spectral intensity, or spectrum, is $S(\omega)$ and the spectral phase is $\phi(\omega)$, the complex electric field is written:

$$E(\omega) = \sqrt{S(\omega)}e^{i\phi(\omega)} \quad (1.1)$$

Very often the spectral phase, $\phi(\omega)$, is expanded in a Taylor series around the center frequency ω_0 because each part has a physical significance.

$$\phi(\omega) = \phi_0 + \phi_1(\omega - \omega_0) + \frac{\phi_2}{2}(\omega - \omega_0)^2 + \frac{\phi_3}{6}(\omega - \omega_0)^3 + \dots \quad (1.2)$$

ϕ_0 is the “absolute” phase: the phase of the carrier wave with respect to the field envelope. ϕ_1 corresponds to a shift in the center frequency of the pulse or, via a Fourier transform, a time shift in the pulse. ϕ_2 is second-order dispersion, called group velocity dispersion (GVD). For a pulse with a Gaussian intensity profile in the time domain, GVD corresponds to a linear shift of frequency (called chirp) with time.

A pulse with positive chirp has a frequency that increases with time; negative chirp has a frequency that decreases with time. Most materials impart positive chirp to a pulse as the pulse propagates through them. The next term, ϕ_3 , is called third-order dispersion (TOD). TOD causes the center frequency to arrive before frequencies on either side of it. This mixing of slightly different frequencies causes a ripple in the time domain. In the time domain, the main pulse will be preceded or followed by smaller pulses, depending on the sign of ϕ_3 .

1.2 History of the measurement problem

When one wants to measure the duration of an event, one has to have a shorter event with which to gate the longer event so that we gain some “snapshots” with which we can see the evolution of the longer event. For example, Q-switched Nd:YAG lasers can produce laser pulses several nanoseconds long that can be measured with fast photodiodes with sub-nanosecond risetimes. Shorter events in the picosecond regime can be measured with streak cameras. But with the advent of broadband dye and Ti:sapphire lasers in the early 1980s, femtosecond pulses became possible. But how do you measure femtosecond pulses without an even faster event to gate it? The obvious answer was to gate the pulse with itself. If one were to break the pulse into two replicas using a Michelson interferometer, a slow detector will record the time-averaged field autocorrelation (or first-order autocorrelation) of the pulse. If the two pulses are delayed with respect to each other by a time τ and we neglect constant terms, the first-order autocorrelation, $\Gamma(\tau)$, will be given by:

$$\Gamma(\tau) = \int_{-\infty}^{\infty} E(t)E^*(t - \tau)dt \quad (1.3)$$

This quantity is also called the interferogram since it records the interference of the fields of the two pulses. The Fourier transform of the interferogram yields the spec-

Chapter 1. Introduction

trum. This is the basis for Fourier-transform spectrometry. But the interferogram gives no information about the spectral phase. It is insufficient to measure a pulse, which requires knowing both the spectrum and the spectral phase.

$$|E(\omega)|^2 = S(\omega) = \mathcal{F} \left\{ \int_{-\infty}^{\infty} E(t)E^*(t - \tau)dt \right\} \quad (1.4)$$

The first attempt to measure ultrafast pulses was the intensity autocorrelation, or second-order autocorrelation. An intensity autocorrelation involves splitting the beam into two parts and mixing them in a nonlinear medium to generate a signal whose electric field in the frequency domain is the convolution in the frequency domain of the electric fields of the two pulses being mixed together. The experimental setup for measuring the autocorrelation is shown in Figure 1.1 [1].

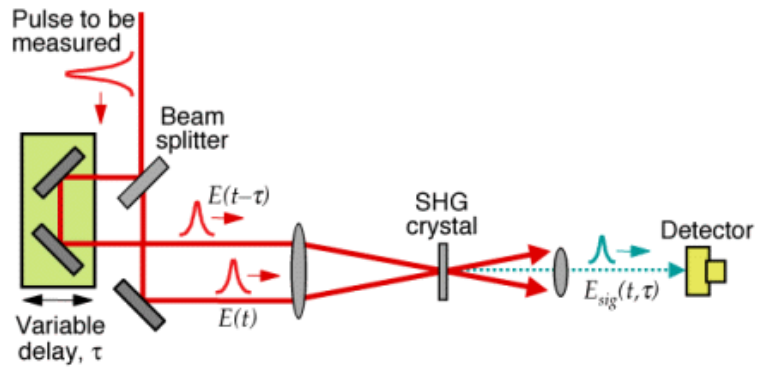


Figure 1.1: Experimental setup for intensity autocorrelation

The nonlinear medium, typically a second-harmonic generation (SHG) crystal, will generate light at twice the frequency as the input beams. The electric field of the this SHG signal is proportional to the two electric fields of the pulses.

$$E_{SHG}(t, \tau) \propto E(t)E(t - \tau) \quad (1.5)$$

The measured intensity autocorrelation is measured by a slow detector which does not resolve the electric field, but the time integral of the magnitude squared. Thus the intensity autocorrelation, $A(\tau)$, is given by:

$$\begin{aligned} A^{(2)}(\tau) &= \int_{-\infty}^{\infty} |E(t)E(t-\tau)|^2 dt \\ &= \int_{-\infty}^{\infty} I(t)I(t-\tau)dt \end{aligned} \tag{1.6}$$

where $I(t) = |E(t)|^2$. Because the intensity autocorrelation is dependent solely on the magnitude squared of a field, it necessarily contains no information about the phase of the field. It has been shown that there are infinitely many fields and intensity profiles that have the same intensity autocorrelations [2]. But although the intensity autocorrelation is incapable of uniquely determining $E(t)$ or even $I(t)$, it does uniquely determine the root-mean-squared pulse width [3].

1.3 Fringe-Resolved Autocorrelation (FRAC)

An improvement upon autocorrelation was pioneered by Jean-Claude Diels in 1983 [4]. Fringe-resolved autocorrelation (FRAC) or interferometric autocorrelation (IAC) involves splitting a pulse into two parts, sending them through a Michelson interferometer, then mixing the two legs in a nonlinear medium and measuring the resultant interferometric intensity profile on a camera. The experimental setup for this is shown below in Figure 1.2 [5].

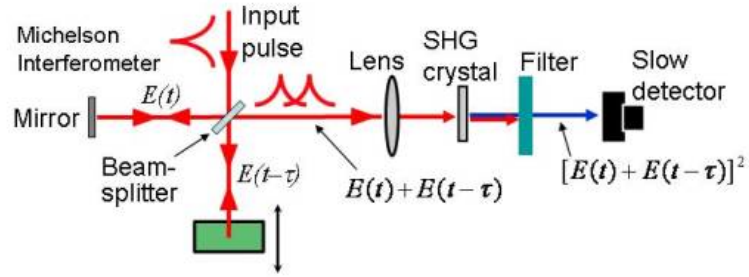


Figure 1.2: Experimental setup for interferometric autocorrelation

The FRAC signal is proportional to the magnitude squared of the sum of the electric fields.

$$\begin{aligned}
 I_{FRAC}(\tau) &= \int_{-\infty}^{\infty} \left| [E(t) + E(t - \tau)] \right|^2 dt \\
 &= \int_{-\infty}^{\infty} \left| E(t)^2 + 2E(t)E(t - \tau) + E(t - \tau)^2 \right|^2 dt \quad (1.7)
 \end{aligned}$$

Expanding out the terms further, we can relate them to intensities and fields of the input beams and group them in the following manner:

$$\begin{aligned}
 I_{FRAC}(\tau) &= \int_{-\infty}^{\infty} I(t)^2 + I(t - \tau)^2 dt \\
 &+ \int_{-\infty}^{\infty} (I(t) + I(t - \tau)) \Re(E(t)E^*(t - \tau)) dt \\
 &+ \int_{-\infty}^{\infty} \Re(E(t)^2 E^*(t - \tau)^2) dt \\
 &+ \int_{-\infty}^{\infty} I(t)I(t - \tau) dt \quad (1.8)
 \end{aligned}$$

The first term is a constant and is therefore centered at frequency 0 when Fourier-transformed into the frequency domain. The second term is like an interferogram, but it is modified by the $(I(t) + I(t - \tau))$ term in front of it. It will be centered at ω_0

Chapter 1. Introduction

in the frequency domain. The third term is an interferogram of the second harmonic and appears centered around $2\omega_0$ in the frequency domain. And the fourth term is an autocorrelation centered around frequency 0 in the frequency domain. Examples of pulses and their FRAC traces are shown below in Figure 1.3, taken from [2, p. 86].

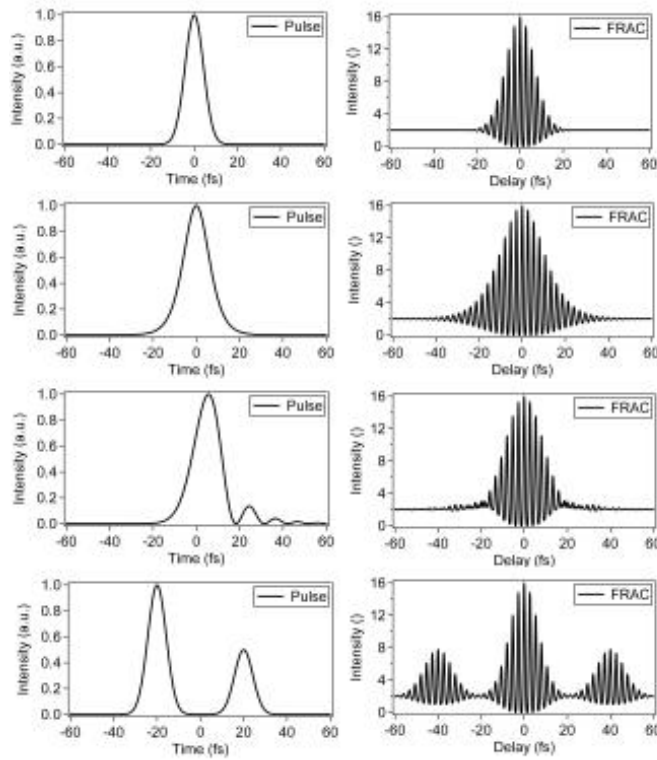


Figure 1.3: Examples of fringe-resolved autocorrelation traces. Top row: a 10 fs Gaussian intensity. Second row: a 7 fs $sech^2$ intensity. Third row: a pulse with considerable TOD. Fourth row: a double pulse.

Naganuma *et al.* showed that knowledge of the fundamental and SHG spectra along with the autocorrelation is a sufficient data set from which to reconstruct a pulse without any assumptions of the pulse shape [6]. Thus FRAC, if combined with

Chapter 1. Introduction

the fundamental spectrum, is a sufficient data set for pulse reconstruction. Naganuma proposed an iterative algorithm to guess a spectral phase for the measured spectrum until a close match is found between the guessed and measured FRAC traces. This technique is not difficult to implement, but it suffers from a time-direction ambiguity and cannot determine distinguish $\phi(\omega)$ from $-\phi(\omega)$. Trebino also questions the accuracy of the technique for very short pulses, since the difference between FRAC traces diminishes as pulse lengths get shorter [2, p.89]. In an effort to retrieve the phase of a pulse without relying on assumptions about the pulse shape, Wolfgang Rudolph *et al.* improved upon FRAC in 1999 by breaking the symmetry of the Michelson interferometer used to delay the two copies of the pulse. One pulse is made to travel through an extra length of dispersive medium (such as fused silica) and the cross correlation between the two legs is generated either in a nonlinear crystal or using a two-photon current detector. This technique is called Phase and Intensity from Cross-correlation And Spectrum Only, or PICASO [7]. It does not have the ambiguity with sign of the chirp that the simpler FRAC had, nor does it need to assume a pulse shape *a priori*. But the dispersion of the material used to unbalance the Michelson interferometer must be known for the technique to work. In 2002, Mansoor Sheik-Bahae and Toshiyuki Hirayama modified FRAC to make the technique more sensitive to chirp [8]. They called their technique MODified Spectrum AutoInterferometric Correlation (MOSAIC). MOSAIC uses the same apparatus as FRAC to collect a second-order interferometric autocorrelation. But in MOSAIC, signal processing removes the components of the trace that are centered at ω_0 . The $2\omega_0$ and autocorrelation components are retained and the $2\omega_0$ component is amplified by a factor of 2. Inverse Fourier transforming this signal in the frequency domain yields the MOSAIC trace in the time domain. Although MOSAIC itself does not fully reconstruct the electric field (although it can if combined with the spectrum), it serves as a real-time diagnostic for low-order dispersion in the beam [9]. Some examples of

pulses with varying amounts of chirp are shown below in Figure 1.4 taken from [8] to show the utility of MOSAIC for diagnosing chirp.

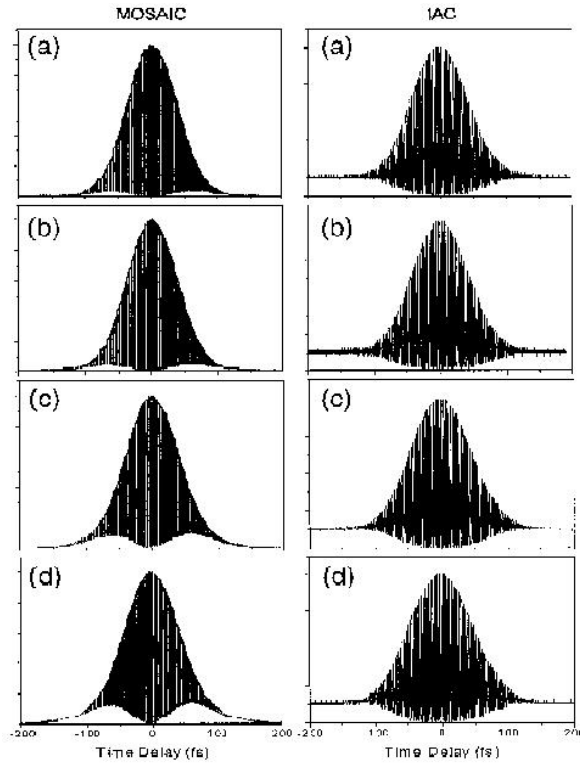


Figure 1.4: Examples of MOSAIC traces compared to FRAC traces. Chirp is varied in each case by making the pulses travel through a 6-mm-thick SiO_2 window for (a) zero, (b) two, (c) three, and (d) five passes.

1.4 Frequency-Resolved Optical Gating (FROG)

It was shown by Ishida *et al.* in 1985 that the electric field of a femtosecond pulse could be fully reconstructed from a spectrally-resolved intensity autocorrelation if the second harmonic spectrum is known for every delay between the two pulses [10].

Chapter 1. Introduction

Although Ishida was the first to make such a measurement, he didn't try to extract intensity and phase information about the pulse. In the early 1990s, Rick Trebino, Daniel Kane, and Ken DeLong used this approach to reconstruct the electric fields of femtosecond pulses [2]. They called the method frequency-resolved optical gating (FROG). FROG involves creating a 2D image of the pulse intensity versus wavelength and delay. Any nonlinear process that can be used for autocorrelation can also be used for FROG, but the most common process is second harmonic generation (SHG) because signal intensities are higher for SHG than for any third-order process (i.e. polarization gating, third harmonic generation, self-diffraction). Figure 1.5 shows how SHG FROG can be implemented in a single-shot configuration [11].

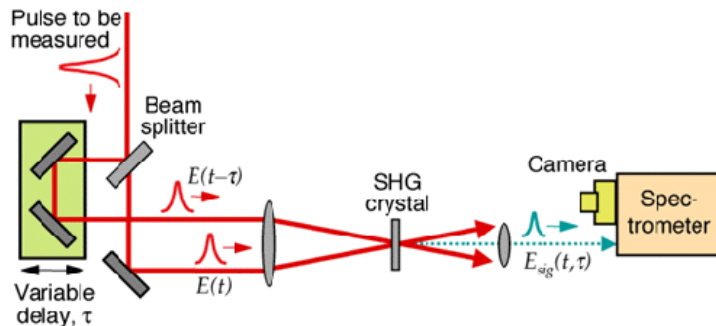


Figure 1.5: Setup for single-shot SHG FROG.

The measured SHG FROG intensity is:

$$I_{FROG}^{SHG}(\omega, \tau) = \left| \int_{-\infty}^{\infty} E(t)E(t - \tau)e^{-i\omega t} dt \right|^2 \quad (1.9)$$

The flowchart for the FROG algorithm has the following steps.

Step 1: The FROG algorithm makes an initial guess for $E(t)$, guessing both an amplitude, $A(t)$, and a phase, $\phi(t)$, for the electric field.

$$E(t) = A(t)e^{i\phi(t)} \quad (1.10)$$

Chapter 1. Introduction

Step 2: It then computes a guessed signal based on whatever nonlinear process is being employed. This is the *mathematical form constraint*. In the case of SHG FROG, it computes the signal field thusly:

$$E_{sig}(t, \tau) \propto E(t)E(t - \tau) \quad (1.11)$$

Step 3: This signal is then Fourier transformed with respect to t to get the signal in the frequency domain:

$$E_{sig}(\omega, \tau) = \int_{-\infty}^{\infty} E_{sig}(t, \tau) e^{i\omega t} dt \quad (1.12)$$

Step 4: This computed signal is in the same domain as the measured signal. Now the algorithm applies a *data constraint*. We replace the guessed amplitude of $E_{sig}(\omega, \tau)$ with the square root of the measured quantity, $\sqrt{I_{FROG}^{SHG}(\omega, \tau)}$, to generate a new signal, $E'_{sig}(\omega, \tau)$ that has the correct amplitude, but not the correct phase.

Step 5: We perform the inverse Fourier transform get back to the time domain from the frequency domain.

$$E'_{sig}(t, \tau) = \frac{1}{2\pi} \int_{-\infty}^{\infty} E'_{sig}(\omega, \tau) e^{i\omega t} d\omega \quad (1.13)$$

Step 6: Integrate the signal over delay to generate $E(t)$ again.

$$E(t) = \int_{-\infty}^{\infty} E'_{sig}(t, \tau) d\tau \quad (1.14)$$

The new $E(t)$ is then used on the next iteration of the cycle, and after a number of iterations, the correct complex electric field is found. Because FROG relies on two dimensional data (intensity vs. wavelength and delay), it is not subject to the ambiguities found in one-dimensional phase retrievals. In general, the two-dimensional phase retrieval problem yields unique answers, but the one-dimensional phase retrieval problem does not [2, p.107]. FROG does contain some so-called “trivial ambiguities” such as not being able to measure the absolute phase, ϕ_0 , nor being able to measure

pulse arrival time (which corresponds via Fourier transform to ϕ_1). SHG FROG also contains a time-direction ambiguity ($E(t) = E^*(-t)$), but third-order FROG traces do not. Also, because FROG collects an N^2 -sized array of data to reconstruct $2N$ points (N amplitude and N phase), the solution is greatly over-determined. This redundancy of data allows the algorithm to diagnose the presence of systematic measurement. SHG FROG traces, for instance, must be symmetric along the delay axis. Asymmetry is an indication of systematic error in SHG FROG. Miscalibrations of the delay or wavelength axis will also lead to large FROG errors.

1.5 Spectral Phase Interferometry for Direct Electric field Reconstruction (SPIDER)

Another elegant method for reconstructing both the amplitude and phase of a pulse is Spectral Phase Interferometry for Direct Electric field Reconstruction (SPIDER), first developed by Chris Iaconis and Ian Walmsley in 1998 [12]. In this technique, an incoming pulse is split into three pulses: A, B, and C. A and B are replicas of the input pulse and have a known delay, τ , of 3-5 picoseconds introduced between them with a delay line or etalon. Pulse C is stretched in time to about 20 picoseconds with a grating stretcher that linearly chirps the pulse, giving a spectral shear of Ω . Then the two replica pulses A and B are nonlinearly mixed with different quasi-monochromatic sections of the spectrally sheared pulse C to produce two pulses, A' and B', that are identical except that B' is frequency-shifted by Ω relative to A'. Then A' and B' are interfered with each other and the interferogram is detected on a slow spectrometer. An experimental setup for the SPIDER technique is shown in Figure 1.6 [13].

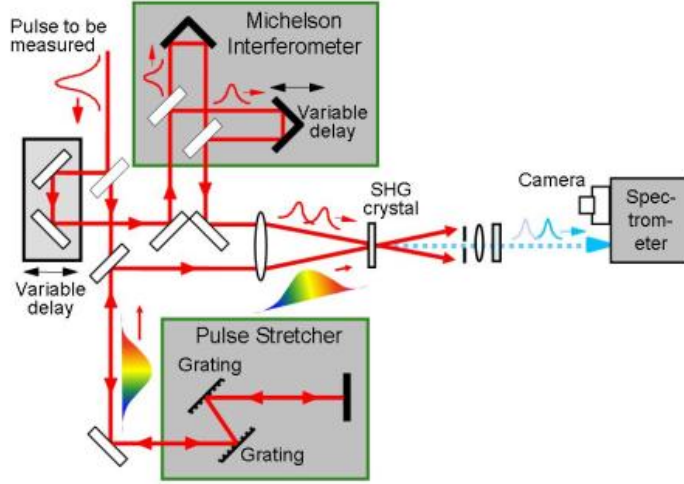


Figure 1.6: Experimental setup for SPIDER.

The fringes resolved by the spectrometer will be given by

$$I_{SPIDER}(\omega) = |E(\omega)|^2 + |E(\omega - \Omega)|^2 + 2 |E(\omega)E(\omega - \Omega)| \cos(\phi(\omega - \Omega) - \phi(\omega) - \tau\omega) \quad (1.15)$$

Fourier transforming these fringes in the frequency domain will yield a DC component and two AC components centered at $-\tau$ and $+\tau$ in time. Next a filter is applied to select only the positive AC component of the Fourier transform. This positive component is then inverse Fourier transformed back to the frequency domain. This yields the phase term $\phi(\omega - \Omega) - \phi(\omega) - \tau\omega$. The $\tau\omega$ term is found by doing a separate SPIDER measurement with the stretched pulse blocked so that the spectral modulation is due only to the the delay in the two replica pulses. When $\tau\omega$ is subtracted, the resulting phase is the phase difference $\phi(\omega - \Omega) - \phi(\omega)$. From this, $\phi(\omega)$ is found by simply phase-wrapping the result whenever it makes a jump of 2π in the phase. The diagram below in Figure 1.7 shows the steps SPIDER uses in reconstructing the phase [14].

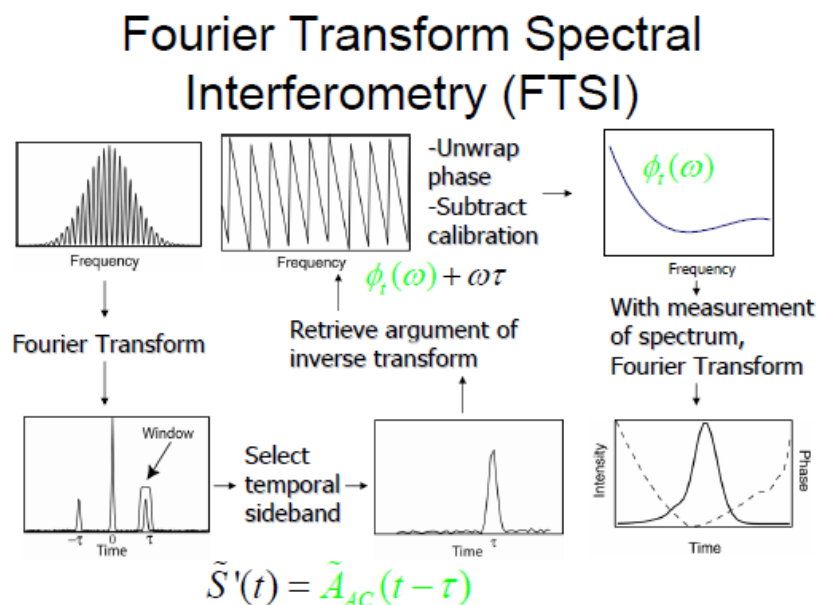


Figure 1.7: Flow chart describing the SPIDER algorithm.

SPIDER has the advantage of being a direct (instead of iterative) method for calculating the phase of a pulse. Furthermore, it is single shot (limited only by the integration time of the spectrometer) and requires a minimum of data to be collected (just one spectrum). However, it is extremely sensitive to alignment of the optics and requires great mechanical stability so the fringes don't wash out. There are also no independent checks in the data to ensure the validity of the measurement. Because it involves the nonlinear mixing of two femtosecond pulses with a stretched picosecond pulse, the nonlinear conversion efficiency is low, requiring higher input energies than other methods.

1.6 SPINS

All the methods listed above that can retrieve the phase of a pulse rely either on spectral interferometry of a nonlinear correlation (FRAC, PICASO, MOSAIC, SPIDER) or spectrally resolving the autocorrelation (FROG). The purpose of this thesis is to explore the possibility of retrieving the phase of a pulse from measuring only the fundamental spectrum along with two nonlinear spectra. For the purposes of this investigation, we record the fundamental, second harmonic, and third harmonic spectra. We start by defining our fundamental pulse as in Equation 1.1:

$$E(\omega) = \sqrt{S_1(\omega)}e^{i\phi_1(\omega)} \quad (1.16)$$

where the subscript 1 denotes the fundamental pulse. The nonlinear SHG and THG pulses will have a similar form:

$$E_{SHG}(\omega) = \sqrt{S_2(\omega)}e^{i\phi_2(\omega)} \quad (1.17)$$

and

$$E_{THG}(\omega) = \sqrt{S_3(\omega)}e^{i\phi_3(\omega)} \quad (1.18)$$

where S_2 and S_3 are the measured SHG and THG spectra, respectively and $\phi_2(\omega)$ and $\phi_3(\omega)$ are the corresponding spectral phases for the SHG and THG pulses. If we assume an instantaneous material response, the nonlinear SHG and THG electric fields in the time domain are proportional to products of the fundamental field in the time domain:

$$E_{SHG}(t) \propto E(t)^2 \quad (1.19)$$

and

$$E_{THG}(t) \propto E(t)^3 \propto E_{SHG}(t)E(t) \quad (1.20)$$

Chapter 1. Introduction

The nonlinear SHG electric field is computed, neglecting constants, as the convolution of the two pulses in the frequency domain:

$$E_{SHG}(\omega) = \int_{-\infty}^{\infty} E(\omega')E(\omega - \omega')d\omega' \quad (1.21)$$

Substituting Equation 1.16 in for $E(\omega)$ in Equation 1.21 we get:

$$E_{SHG}(\omega) = \int_{-\infty}^{\infty} \sqrt{S_1(\omega')S_1(\omega - \omega')}e^{i(\phi(\omega')+\phi(\omega-\omega'))}d\omega' \quad (1.22)$$

Thus, the SHG spectrum is dependent upon the fundamental spectrum and phase by:

$$S_2(\omega) = \left| \int_{-\infty}^{\infty} \sqrt{S_1(\omega')S_1(\omega - \omega')}e^{i(\phi(\omega')+\phi(\omega-\omega'))}d\omega' \right|^2 \quad (1.23)$$

Similarly, because of Equation 1.20 which shows that the THG field is proportional to the SHG field times the fundamental field in the time domain, we can write the THG field as the convolution of the SHG field with the fundamental field in the frequency domain:

$$E_{THG}(\omega) = \int_{-\infty}^{\infty} E_{SHG}(\omega')E(\omega - \omega')d\omega' \quad (1.24)$$

Then the THG spectrum can be written in terms of the fundamental spectrum and phase as follows:

$$S_3(\omega) = \left| \int_{-\infty}^{\infty} E_{SHG}(\omega')E(\omega - \omega')d\omega' \right|^2 \quad (1.25)$$

In the SPINS retrieval algorithm, a pulse is defined by the measured fundamental spectrum times a spectral phase, as in Equation 1.16. The initial phase of the pulse is guessed. The fundamental field $E(\omega)$ is Fourier transformed to $E(t)$ and the trial second and third harmonic fields are generated via Equations 1.19 and 1.19. Instead of using a $\chi^{(3)}$ process such as THG, a cascaded $\chi^{(2)}$ process could be used instead. For instance, instead of generating the third harmonic directly, the second harmonic could be mixed with the fundamental to get either THG or downconverted

Chapter 1. Introduction

via difference frequency generation (DFG) back to the fundamental frequency. Mathematically, the THG process is the same; the THG electric field is proportional to the input field cubed. $E_{THG}(t) \propto E(t)^3$. But with DFG, the electric field is at the same frequency as the initial field, so $E_{DFG}(t) \propto E(t)^2 E(t)^*$. The advantage of cascaded $\chi^{(2)}$ is greater conversion efficiency of the fundamental beam to the third-order beam. The major disadvantage is added experimental complexity, as the SHG and fundamental beams have to be overlapped in time using a delay line. Plus, in the case of using DFG to get a nonlinear signal at the fundamental frequency, the beams need to be mixed in a non-collinear geometry so the DFG signal can be separated from the original fundamental. These fields are then inverse Fourier transformed back to the frequency domain and the magnitude squared of the field is the trial SHG or THG spectrum, $S_{SHG}^{trial}(\omega)$ and $S_{THG}^{trial}(\omega)$. An error function, Δ , is computed as a quadratic root-mean-square deviation between the trial and measured spectra with N points each:

$$\Delta = \left[\frac{1}{N} \left[\sum_{i=1}^N \left[(S_{SHG}^{trial}(\omega_i) - S_{SHG}^{measured}(\omega_i))^2 + (S_{THG}^{trial}(\omega_i) - S_{THG}^{measured}(\omega_i))^2 \right] \right] \right]^{.5} \quad (1.26)$$

The phase is defined in the frequency domain using the convention given in Equation 1.2. The coefficients of each term of the expansion are varied iteratively until a minimum in the error function is achieved. Because SPINS involves only the direct generation of second and third harmonics, there is no delicate time overlapping between the pulses. Since there is no interferometry involved, the experimental setup is robust and not sensitive to small changes in path length. Depending on the wavelengths used, it is at least theoretically possible for all three spectra to be measured with the same spectrometer. SPINS is also the only one of these techniques that is robust enough to theoretically work with an input pulse that has a poor-quality wavefront, although this claim was not tested.

Chapter 2

Algorithm Development

2.1 Uniqueness of solution

The investigation into the efficacy of the SPINS technique begins by studying whether or not it will lead to unique solutions. To test this, a sample pulse is generated with a known spectrum and phase. The phase is restricted to GVD and TOD terms only, i.e. $\phi(\omega) = \phi_2(\omega - \omega_0)^2 + \phi_3(\omega - \omega_0)^3$. In our case, a *sech*² spectrum was modified so that it became asymmetric and values of GVD and TOD were chosen so that the generated phase caused the pulsewidth by about 40 percent over the transform limit. The time domain intensities of the two pulses are shown below in Figure 2.1.

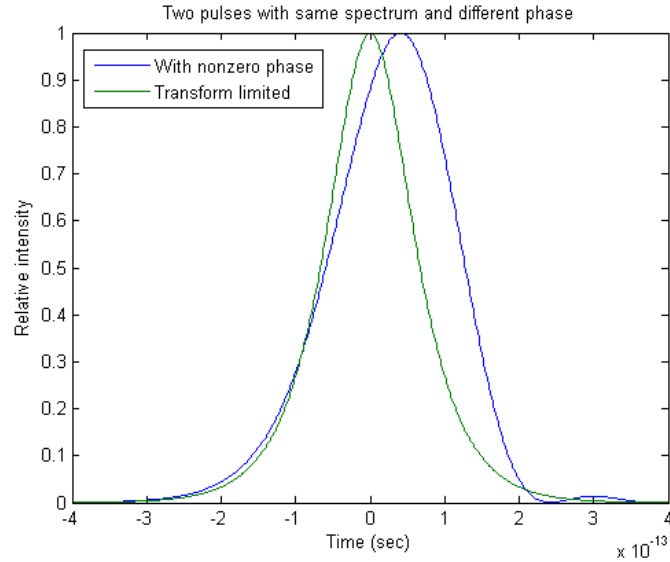


Figure 2.1: Pulse in time domain with $GVD = 50,000 \text{ fs}^2$ and $TOD = -10,000,000 \text{ fs}^3$ compared to transform-limited pulse.

Errors, as defined in Equation 1.26, were computed for pulses with different values of GVD and TOD and those errors were plotted versus against the GVD and TOD values to generate an error map. For the example shown below in Figure ??, the known GVD is $50,000 \text{ fs}^2$ and TOD is $-10,000,000 \text{ fs}^3$. The algorithm did converge to a solution at the known values of GVD and TOD. It also converged to a solution at the opposite of those values. This ambiguity shows that the same nonlinear spectra are generated with the phase $\phi(\omega)$ as with $-\phi(\omega)$. This corresponds to a direction-of-time ambiguity. The 3D graph of the error map shown below in Figure 2.3 makes the convergence to the two phase points more obvious.

Chapter 2. Algorithm Development

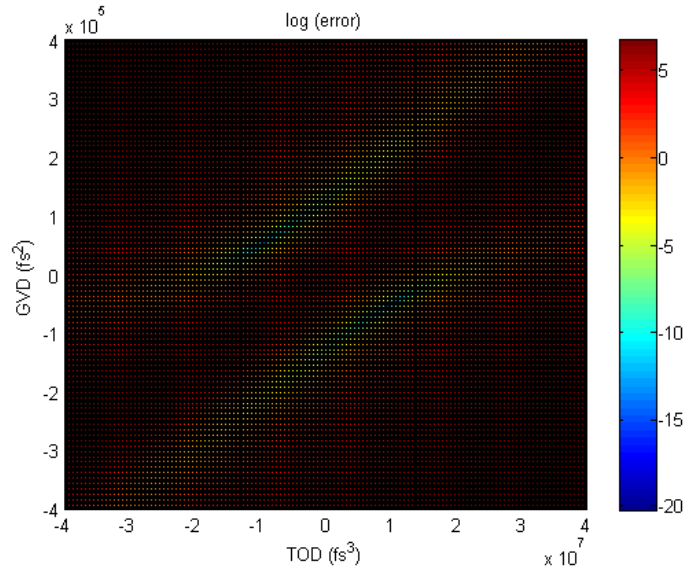


Figure 2.2: Error map for pulse with known $GVD = 50,000 \text{ fs}^2$ and $TOD = -10,000,000 \text{ fs}^3$. The log of the error is plotted. Solutions are at blue points.

Although this is not a conclusive proof of the uniqueness of the solution for a general phase, it does show that the solution is essentially unique when spectral phase is confined to GVD and TOD only.

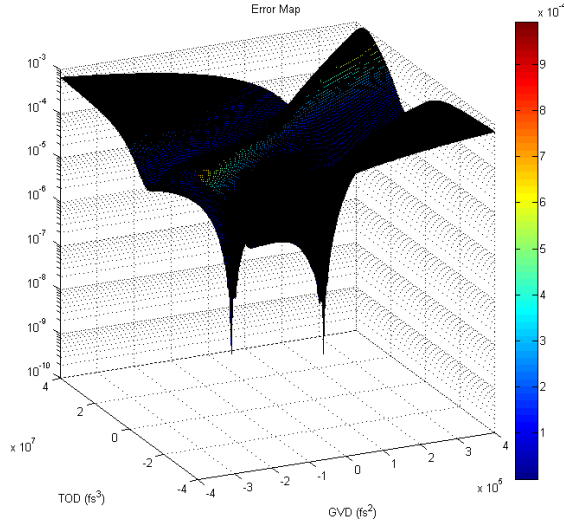


Figure 2.3: 3D Error map for pulse with known $\text{GVD} = 50,000 \text{ fs}^2$ and $\text{TOD} = -10,000,000 \text{ fs}^3$. Note the two points where the error is exceedingly small. These are the two solutions.

2.2 Sensitivity to phase

Another important consideration in assessing the versatility of a femtosecond pulse measurement technique is its sensitivity to phase. How does the sensitivity of SPINS compare to FROG? Using pulses with the same spectrum above, the phase was changed by adding a fourth order dispersion (FOD) term to the Taylor series expansion of the phase. GVD and TOD remained the same, but a FOD coefficient of $-100,000,000 \text{ fs}^4$ modified the phase. This phase caused the pulse to be 43% longer in the time domain compared to the transform-limited pulse, as seen in Figure 2.4. The SHG and THG spectra as well as FROG traces were simulated and compared with each other. The FROG traces were generated via Equation 1.12 using time-domain data that was truncated to 2^{10} points from the original 2^{16} points. This was done

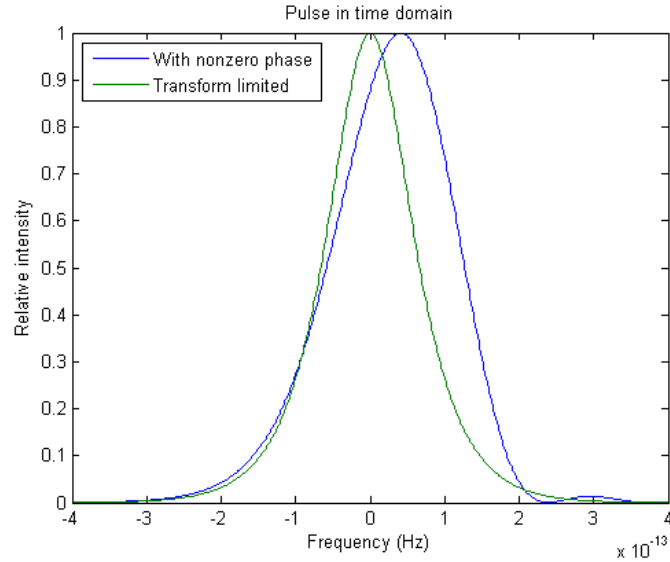


Figure 2.4: Pulse in time domain with $GVD = 50,000 fs^2$, $TOD = -10^7 fs^3$, and $FOD = -10^8 fs^4$ compared to transform-limited pulse.

solely because Matlab could not handle an array size necessary to accommodate the points necessary to maintain that same resolution in the frequency domain. Since the time-domain data was truncated to 1/64 of its original value, the frequency data is necessarily coarsened by a factor of 64. This must be kept in mind when comparing the two techniques. The square of the differences are summed over frequencies in the case of the SHG and THG spectra. The square of the differences in the FROG images are summed over frequencies and delay, since FROG data are 2D spectrograms. In neither case was the difference divided by the number of points because of the different frequency resolutions of the spectra compared to the FROG data. The spectra and FROG images for the two pulses are shown below.

Chapter 2. Algorithm Development

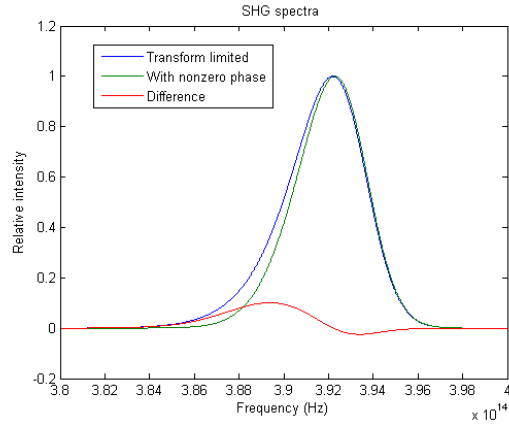


Figure 2.5: Plot showing the differences in SHG spectra between a transform-limited pulse and one with phase that causes a 43% stretching in time domain

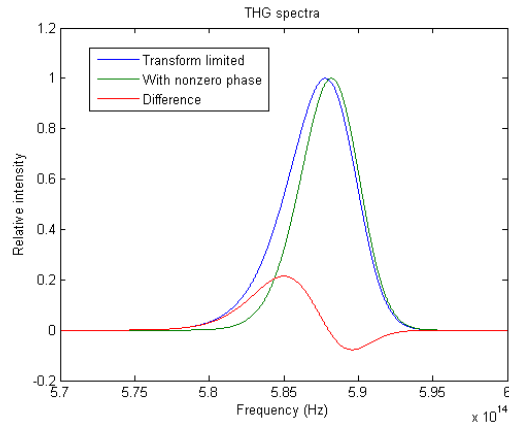


Figure 2.6: Plot showing the differences in THG spectra between a transform-limited pulse and one with phase that causes a 43% stretching in time domain

Chapter 2. Algorithm Development

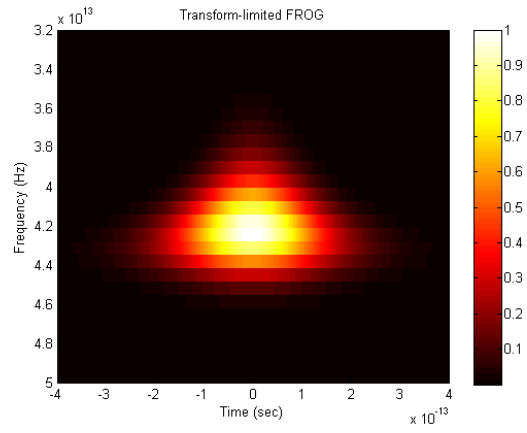


Figure 2.7: Transform-limited FROG image

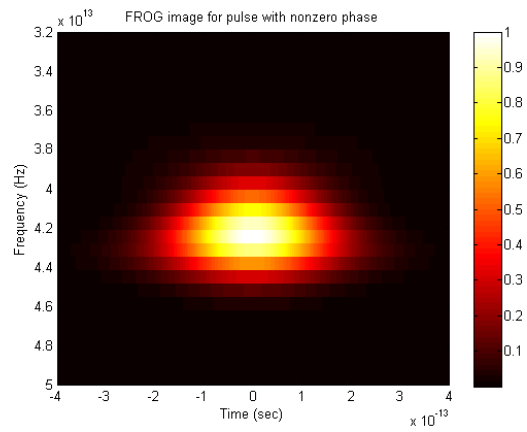


Figure 2.8: FROG image of pulse with non-zero phase

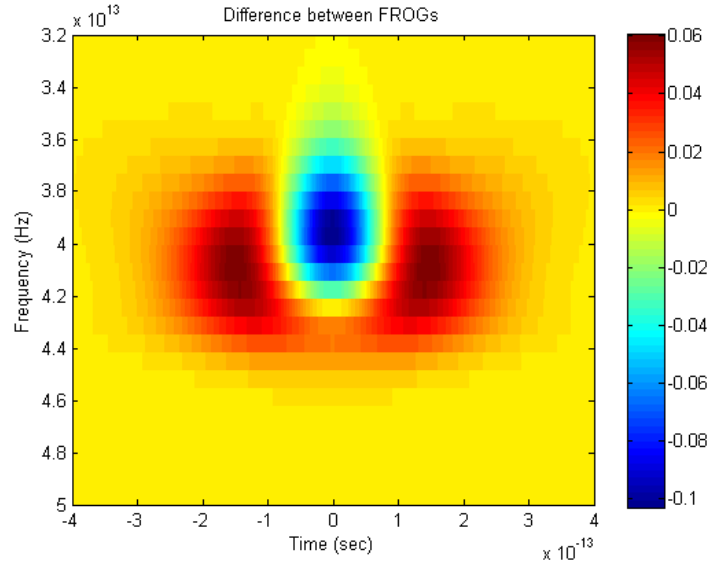


Figure 2.9: Difference between the transform-limited and non-zero phase FROG images

One way of estimating the sensitivity to phase is to compare the peak-to-peak differences of the spectra. The peak-to-peak difference between the transform limited spectra and the other spectra were 12.6% for the SHG spectra, 29.2% for the THG spectra compared to a 16.3% peak-to-peak difference in the FROG images. Given this metric, SPINS is seen to be of comparable sensitivity to FROG.

2.3 Resiliency to noise

Every real measurement will have random noise. FROG traces can have random noise introduced by dark current in the CCDs or stray light in the spectrometers. However, the FROG retrieval algorithm is robust and random noise does not affect it greatly since random noise will rarely appear in such a pattern as to cause the algorithm

Chapter 2. Algorithm Development

to mistake the actual pulse for another pulse. In the case of SPINS, much less data is collected than in FROG and therefore there is not the self-correcting redundancy inherent to FROG. The measured spectra in SPINS have the same sources of noise as FROG traces: dark current in the detector arrays and stray light in the spectrometers. We next explore how much random noise the three spectra can have before the SPINS retrieval algorithm fails to retrieve the known phase.

Using the same pulse with non-zero phase described earlier, we first add random noise to the fundamental spectrum. The SHG and THG spectra are then generated from this noisy spectrum with a well-defined phase. Next, different random noise of the same magnitude as the first is added to the SHG and THG spectra. The retrieval algorithm is run using a simplex method to find the known coefficients of the GVD, TOD, and fourth order dispersion (FOD) of the phase. With the error defined as in Equation 1.26, the algorithm was able to retrieve the phase when noise with a magnitude of 0.8% of the maximum signal was introduced.

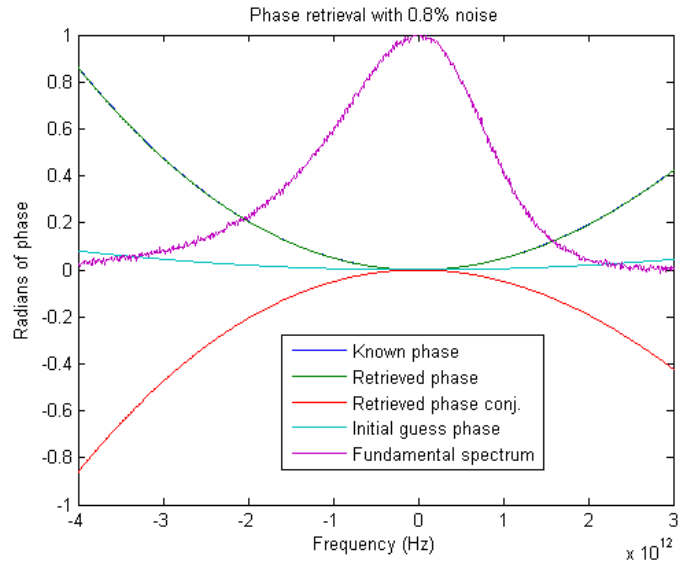


Figure 2.10: Phase retrieval using simplex method with 0.8% noise. Known phase (dark blue) and retrieved phase (green) are almost indistinguishable.

As seen above in Figure 2.10, the retrieval algorithm converged to the known phase. The retrieved and computed SHG and THG spectra with 0.8% noise are shown below in Figures 2.11 and 2.12.

Chapter 2. Algorithm Development

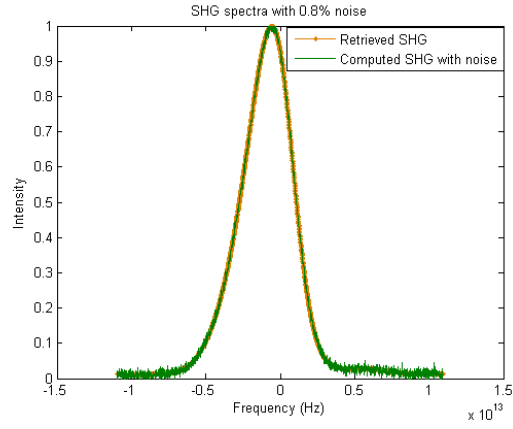


Figure 2.11: Retrieved (orange) and computed (green) SHG spectra with 0.8% noise.

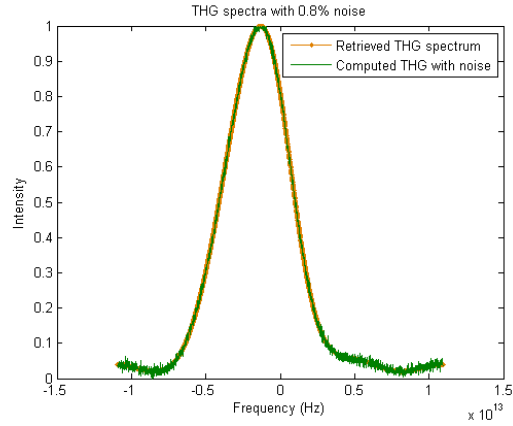


Figure 2.12: Retrieved (orange) and computed (green) THG spectra with 0.8% noise.

Chapter 2. Algorithm Development

However, when the noise level is increased to 1 percent, the retrieval algorithm fails to retrieve the known phase. As seen in Figure 2.13 below, the known phase (dark blue) and retrieved (red) phases begin to deviate noticeably in the wings of the spectrum.

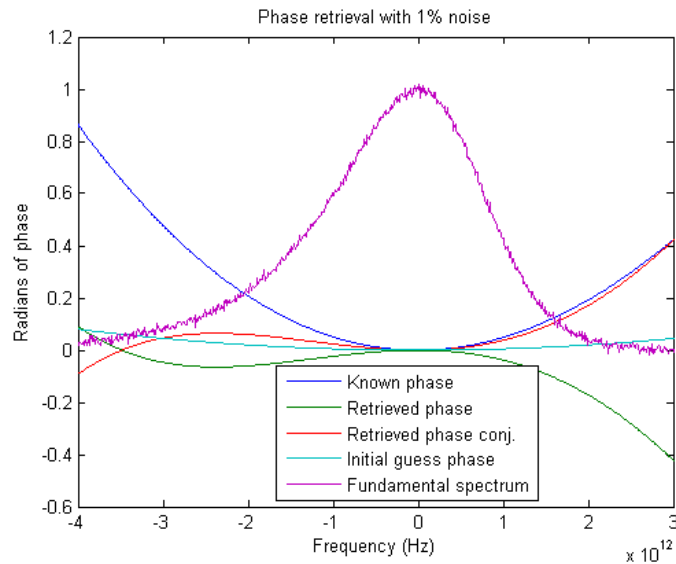


Figure 2.13: Phase retrieval using simplex method with 1 percent noise. Known phase (dark blue) and conjugate of the retrieved phase (red) deviate noticeably in the pulse wings.

The retrieved nonlinear spectra match their computed counterparts well when the intensity is high, but not in the wings where it is not, as seen in Figures 2.14 and 2.15 below.

Chapter 2. Algorithm Development

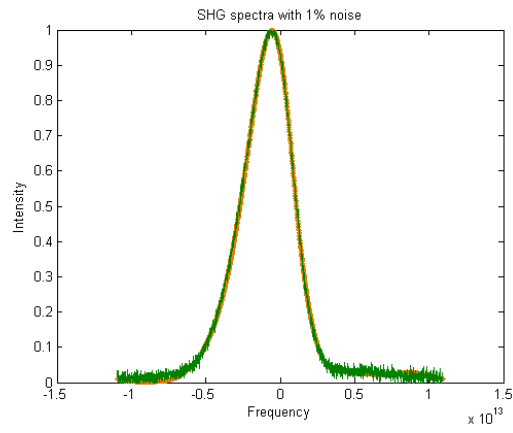


Figure 2.14: Retrieved (orange) and computed (green) SHG spectra with 1 percent noise.

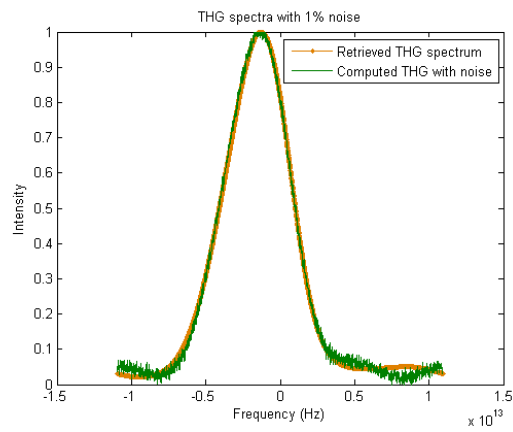


Figure 2.15: Retrieved (orange) and computed (green) THG spectra with 1 percent noise.

Chapter 2. Algorithm Development

To address this problem, the error function was modified to give more weight to the wings of the pulse. This is done by multiplying the square of the difference in the spectra by the absolute value of the frequency (assuming the center frequency is 0). The modified error signal is given by Equation 2.1.

$$\Delta_{mod} = \left[\frac{1}{N} \sum_{i=1}^N \left[(S_{SHG}^{Strial}(\omega_i) - S_{SHG}^{measured}(\omega_i))^2 |\omega_i| + (S_{THG}^{Strial}(\omega_i) - S_{THG}^{measured}(\omega_i))^2 |\omega_i| \right] \right]^{.5} \quad (2.1)$$

With this modification to the error signal, the retrieval algorithm was able to retrieve the phase with 1.1 percent noise in the spectra, a 37.5 percent improvement. The successful retrieval is shown below in Figure 2.16. The known phase, the hardly visible dark blue line, is virtually identical to the conjugate of the retrieved phase, the red line.

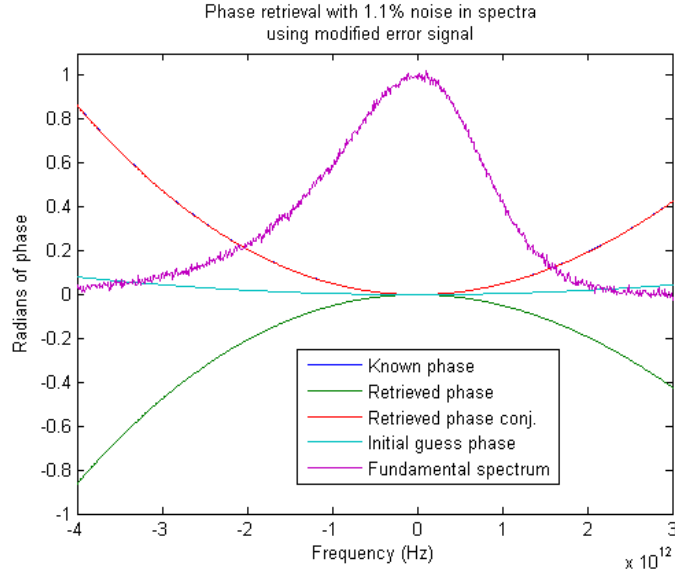


Figure 2.16: Phase retrieval using simplex method with 1.1% noise. Known phase (dark blue, hardly visible) and conjugate of the retrieved phase (red) are almost identical.

Chapter 2. Algorithm Development

As seen below in Figures 2.17 and 2.18, the retrieved SHG and THG spectra fit the computed spectra much better with the modified error function which weights points farther from the center frequency more than with the original error function.

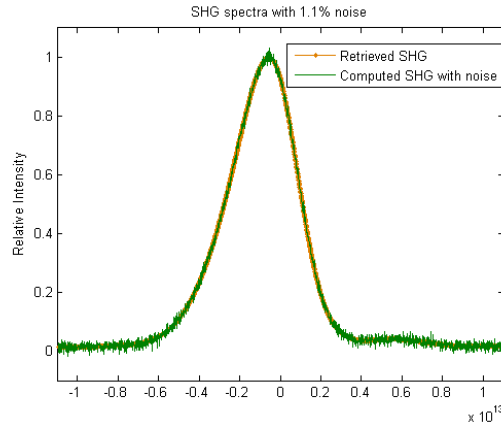


Figure 2.17: Retrieved (orange) and computed (green) SHG spectra with 1.1% noise.

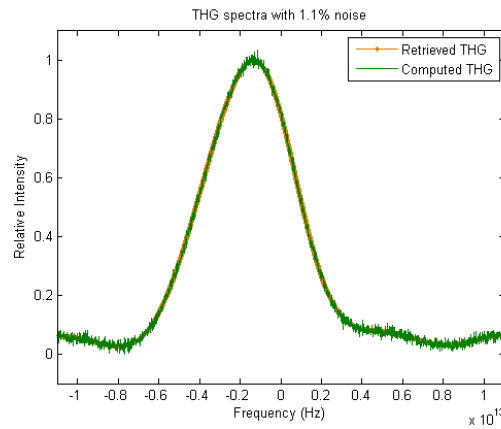


Figure 2.18: Retrieved (orange) and computed (green) THG spectra with 1.1% noise.

Chapter 3

Experimental Validation

3.1 Purpose

Having resolved that the retrieval algorithm can retrieve a known phase based on a 3-term Taylor expansion of the phase around the center frequency (GVD, TOD, and FOD) using a simplex search method, we test the algorithm against real data obtained from experiment.

3.2 Experimental Setup

A 10 Hz rep rate optical parametric chirped pulse amplifier (OPCPA) laser was used in this experiment because the 10 Hz rep rate made it easy to externally trigger the spectrometers and to obtain single-shot data. Also, the third harmonic generation efficiency in air is particularly good at 1550 nm, making it easy to generate the non-linear spectrum that will have the lowest signal. The laser produces 170 fs pulses tunable around 1550 nm wavelength with energies of about 5 mJ. The Martinez-

Chapter 3. Experimental Validation

designed pulse compressor utilizes a retroreflector mounted on a translation stage to vary the the pulsewidth by changing the spacing between the gratings. The experimental setup for the SPINS measurement is quite simple and is shown below in Figure 3.1.

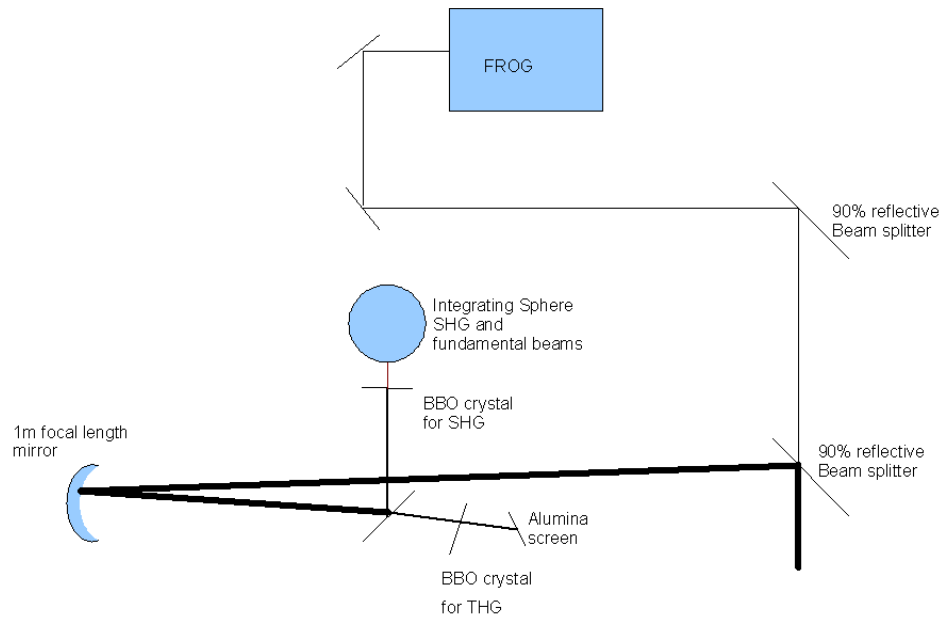


Figure 3.1: Experimental setup for SPINS.

The majority of the beam is reflected off a 90 percent reflective beam splitter (CVI BS1) onto a 1 meter focal length gold mirror which begins to focus the beam. A femtosecond autocorrelating beam splitter (CVI FABS 1550) splits the converging beam into two legs: one to generate SHG and the other to generate THG. A BBO crystal angle-tuned to phase match SHG or THG is placed well upstream of the focus to minimize the onset of self-phase modulation. An integrating sphere behind the SHG BBO crystal collected light for the fiber-coupled SHG spectrometer (an Ocean Optics HR2000) and the fundamental imaging spectrometer (an Acton AR150 with

a Sensors Unlimited SU320 InGaAs camera). A small alumina disk placed just after the THG BBO crystal provided a surface for diffuse reflection into a 1 mm diameter fiber that coupled into an Ocean Optics USB2000 spectrometer. The 10 percent of the beam that passed through the original beam splitter was reflected off another 90 percent reflective beam splitter, through two lenses that served as a telescope, off two more dielectric mirrors and into a SHG FROG.

3.3 Procedure

The experimental procedure involved measuring single-shot spectra of the fundamental, second harmonic, and third harmonic along with a FROG trace for comparison to an established phase-retrieval method. The laser was tuned to produce 170 fs pulses with about 5 mJ per pulse and a center wavelength of 1540 nm. The compressor stage was scanned through positions near optimal compression to vary the group velocity dispersion (GVD) component of the spectral phase. At each compressor position, data were taken both with and without a thick piece of fused silica glass in the beam prior to the first beam splitter. The additional fused silica adds third-order dispersion (TOD) to the spectral phase.

3.4 Results

As the compressor stage moved and the amount of GVD in the phase changed, it was obvious that both the shape and relative intensity of the SHG and THG spectra changed, as expected. However, due to instability of the laser energy shot-to-shot and instability of the fundamental spectrum, it is difficult to observe any general trend in how GVD affects the nonlinear spectra by eye on this laser. Figure 3.2 below shows

Chapter 3. Experimental Validation

the great shot-to-shot variability in the fundamental spectrum of this OPCPA laser.

The variability of the fundamental spectrum causes variability in the nonlinear

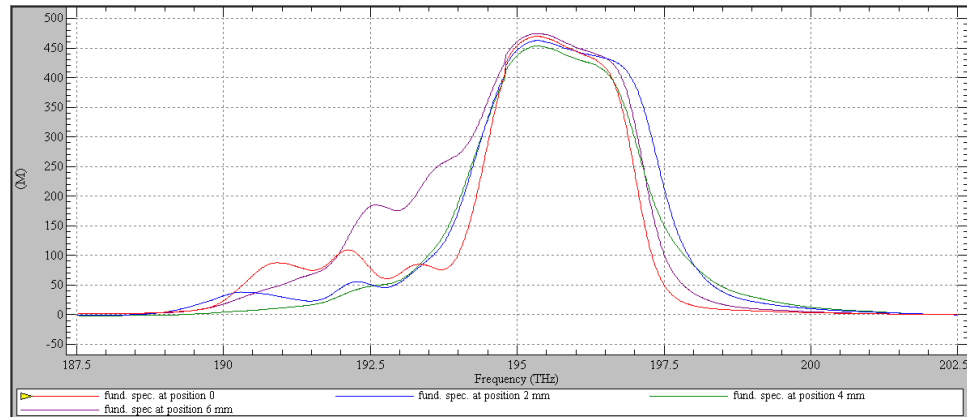


Figure 3.2: Fundamental spectra as recorded for 4 different shots

spectra as well. The change in the nonlinear spectra in the four shots shown below in Figures 3.3 and 3.4 are from both changes in GVD between the shots as well as variability of the fundamental spectrum. Instability of the laser should not cause a

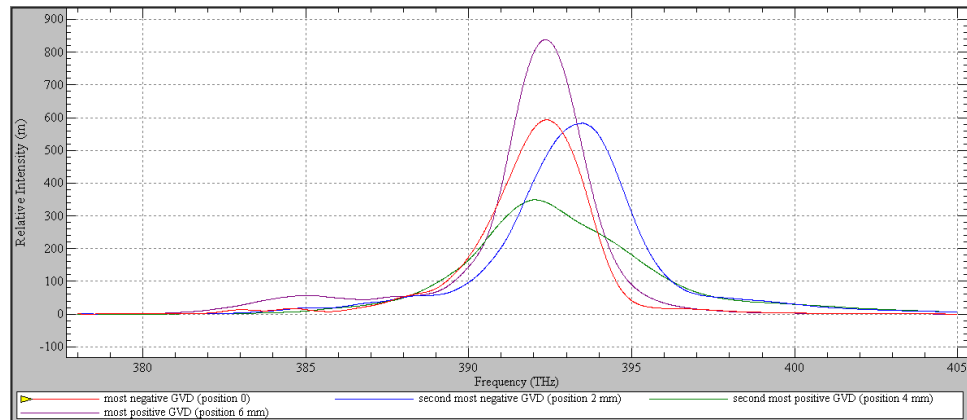


Figure 3.3: SHG spectra as recorded for 4 different shots with different GVD.

Chapter 3. Experimental Validation

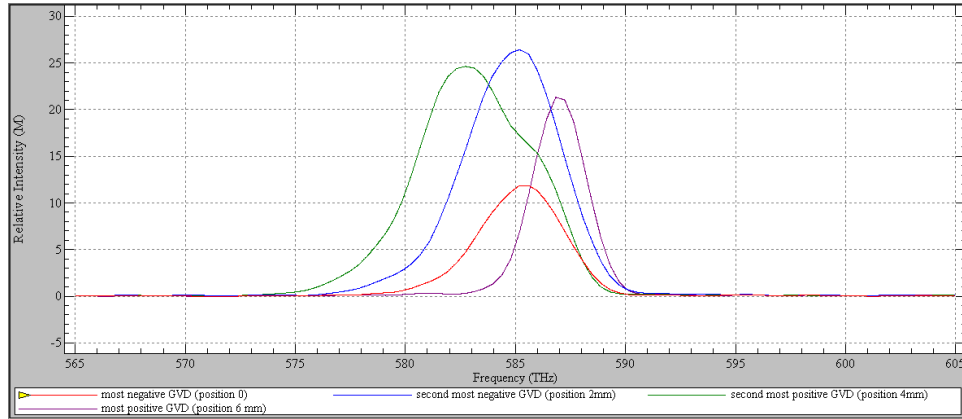


Figure 3.4: THG spectra as recorded for 4 different shots with different GVD.

problem with retrieving the phase of a pulse as long as all measurements were taken on the same pulse. However, post-processing of the data indicated that the fundamental spectrum as measured by the Acton imaging spectrometer was considerably different than the spectrum retrieved by the FROG, as seen in Figure 3.5. The cause of this error is unlikely to be a problem with the FROG as the FROG reconstructions had a low error, indicating that they converged to a solution. Miscalibrations of the FROG would result in higher FROG error. Since the spectrum measured by the imaging spectrometer is much wider, it is likely caused by optical parametric gain (OPG) in the amplifier crystals. These crystals are thin enough to match more bandwidth than the 1550 nm seed laser produces. OPG would amplify whatever vacuum photons could be phase matched with the crystals. The OPG spectrum would therefore be wider than the seed spectrum that is amplified, but would have a pulsewidth comparable to that of the pump laser, about 300 ps. After traveling through the pulse compressor, the OPG would remain uncompressed while the amplified seed would be compressed to hundreds of femtoseconds. But the imaging spectrometer does not care about the pulse duration; it simply counts whatever photons are at each wavelength, regardless

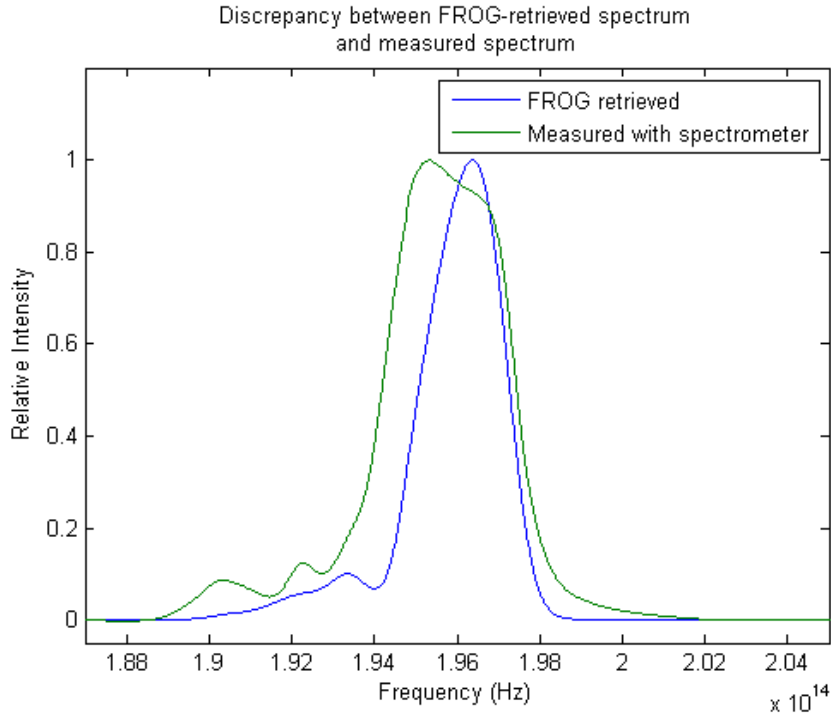


Figure 3.5: Fundamental spectra as recorded by the imaging spectrometer (green) and retrieved by FROG (blue).

of pulsewidth. The FROG is not afflicted by this problem since it retrieves the fundamental spectrum from looking at the SHG spectrum. The SHG spectrum is intensity dependent and the OPG will make a negligible contribution to the SHG spectrum. Thus FROG in this case more reliably measures the fundamental spectrum than does the imaging spectrometer.

To test the SPINS algorithm with real data, we substitute the FROG-retrieved fundamental spectrum for the measured fundamental spectrum and keep the measured SHG and THG spectra. The input spectra are shown below in Figure 3.6 and the measured FROG image is shown in Figure 3.7.

Chapter 3. *Experimental Validation*

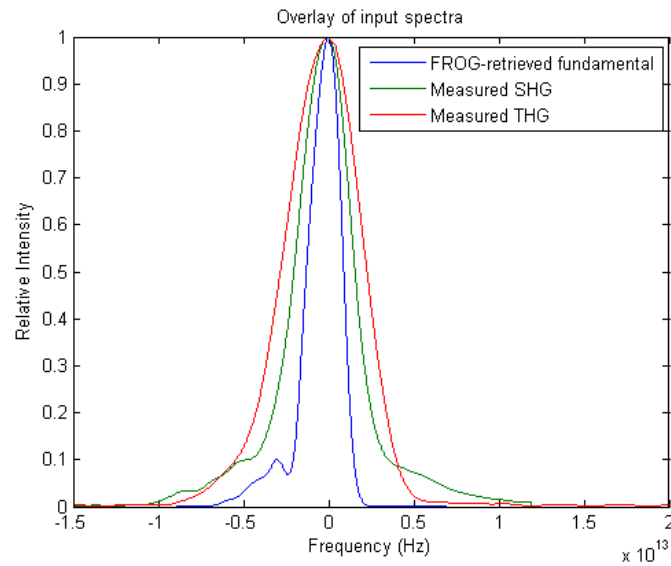


Figure 3.6: Fundamental, SHG, and THG spectra used as input to SPINS algorithm.

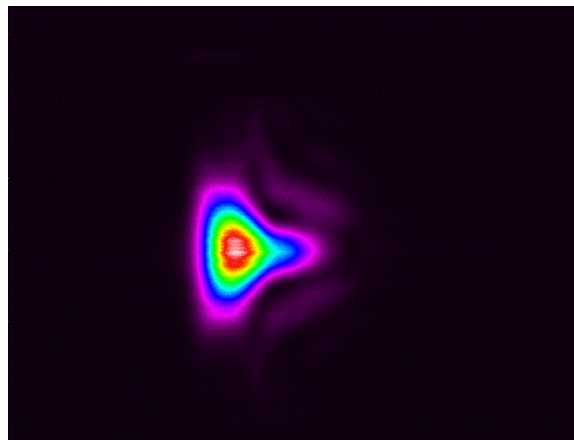


Figure 3.7: Measured FROG image. Wavelength is on the horizontal axis and delay is on the vertical axis.

The retrieved FROG error was 0.00203854. An error of 0.01 is considered acceptable and 0.005 is good in practice. There are no units show for the axes be-

cause they are scaled in post-processing. The results of the SPINS phase retrieval are seen in Figure 3.8. The SPINS-retrieved phase differs noticeably from the the FROG-retrieved phase. Plotting the SHG and THG spectra computed from the

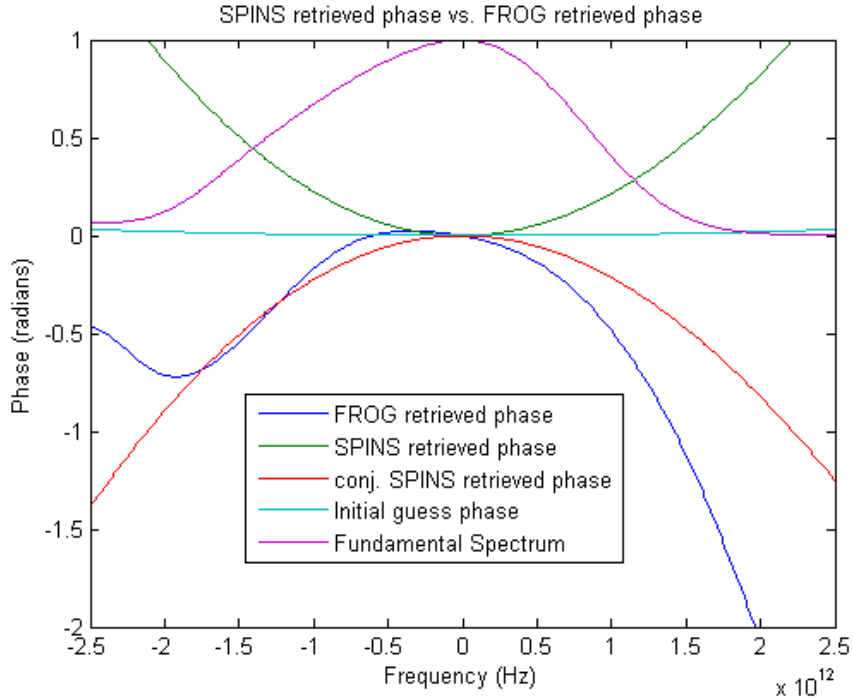


Figure 3.8: Comparison of SPINS and FROG phase retrievals. SPINS-retrieved phase (red) differs markedly from FROG-retrieved phase (dark blue).

FROG-retrieved phase and SPINS-retrieved phase is useful in diagnosing the discrepancy between the two methods. An overlay of the measured, SPINS-retrieved, and FROG-retrieved SHG spectra is shown in Figure 3.9. Neither phase retrieval method generates an SHG spectrum that has the pedestal that is seen in the measured SHG spectrum. This could be indicative of measurement problem with the SHG spectrum. The corresponding THG spectra are plotted in Figure 3.10. There is good agreement between the FROG-retrieved THG spectrum and the measured THG spectrum.

Chapter 3. Experimental Validation

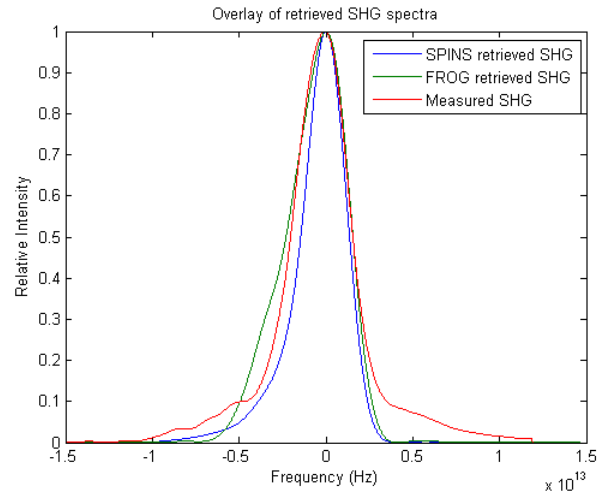


Figure 3.9: Comparison of SHG spectra: SPINS-retrieved (blue), FROG-retrieved (green) and measured (red).

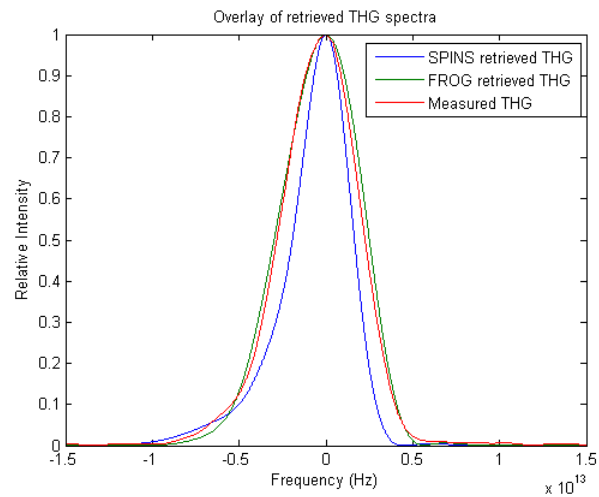


Figure 3.10: Comparison of THG spectra: SPINS-retrieved (blue), FROG-retrieved (green) and measured (red).

Chapter 3. Experimental Validation

Since there is good agreement between the FROG-retrieved THG spectrum and the measured spectrum and a low FROG error, it is reasonable to conclude that the FROG is working correctly. It is not known why the SHG FROG spectrum does not match the SHG spectrum measured with the fiber-coupled spectrometer. The wings seen on the measured SHG spectrum could be due to the broadband OPG from the amplifier crystals. Although the pulsewidth of the OPG is on the order of 300 ps, the BBO crystal used to generate the SHG is about 1mm thick, which might allow measurable conversion of the OPG to its second harmonic. Perhaps the reason it would not show up in the FROG trace is because it uses a thinner crystal and the input intensity is lower by several orders of magnitude.

Chapter 4

Conclusion

It was demonstrated using machine-generated spectra and phases that the SPINS technique can be used to retrieve the phase of pulses using only the fundamental, SHG, and THG spectra as input parameters. The technique contains a time-reversal ambiguity, but other ambiguities arising from using only the low-order Taylor approximations to the phase are seen to describe the same phase when looking at the region that matters, i.e. frequencies where the spectral intensity is non-negligible. The retrieval algorithm can retrieve the phase with 0.8% noise in all three spectra. Weighting the error function by the absolute value of the frequency (assuming a carrier frequency of 0) improves the performance of the algorithm, allowing retrieval with 1.1% noise in the spectra. The technique is simple to implement, requiring only three spectrometers, and simple to align since there are no concerns with spatial and temporal overlap of beams. Also, since the technique does not attempt to map pulse delay onto position in the crystal like other single-shot techniques, it is potentially insensitive to wavefront distortions.

Some experimental concerns became apparent while trying to collect the three spectra. Third harmonic can be generated in air quite easily with 1550 nm pulses.

Chapter 4. Conclusion

However, as the beam focuses in air to get the intensities high enough to generate third harmonic, another $\chi^{(3)}$ process, self-phase modulation (SPM), is also occurring. SPM broadens the fundamental wavelength and this broadened fundamental also converts to third harmonic. Thus the third harmonic spectra generated by focusing a beam in air is different from one that is generated in a nonlinear crystal placed before the focus that is phase-matched to preferentially yield the third harmonic. Ideally, THG should be generated by a phase-matched crystal in vacuum to minimize SPM.

1550 nm light cannot be detected with silicon detectors. Thus the imaging spectrometer used to measure the fundamental spectrum uses an InGaAs camera. These InGaAs cameras have a non-uniform response pixel to pixel that must be calibrated out. All the spectrometers, regardless of material, should have their spectral responses calibrated. This is essential when trying to fit the shape of a computed spectrum to that of a measured one.

Chapter 5

Future Work

The SPINS algorithm as it is now written attempts to retrieve the coefficients of the GVD, TOD, and FOD Taylor series expansion of the phase. Many pulses are afflicted with phases that cannot be adequately described using only these three terms. It would be preferable to use more terms or let every point in the phase vary independently of the others. Allowing all the points to vary independently greatly increases the computational demands. This was accomplished, however, using a quasi-Newton algorithm being fed noiseless spectra and an initial guess for the phase that was not greatly different than the known phase. It failed when the initial guess varied too much from the known phase, showing the lack of robustness of the quasi-Newton method. A genetic algorithm proved to be quite insensitive to initial guesses, but was computationally expensive. Furthermore, the genetic algorithm in Matlab seems to have a maximum number of variables that it will optimize and it was not enough to allow every point of the phase to float. The simplex method proved to be a good compromise between robustness and computational time. Future work could include using a simplex method or genetic algorithm to retrieve the phase while letting all the points in the phase float instead of expressing the phase in terms of a Taylor

Chapter 5. Future Work

expansion. This will likely have to be programmed in a language other than Matlab. The 1550 OPCPA laser turned out to be a poor choice for testing the SPINS algorithm owing to the problems in measuring the fundamental and SHG spectra caused by the OPG. Future validation should be carried out on a Ti:sapphire laser system at 800 nm. A laser operating nominally at 800 nm will have SHG at 400 nm and THG at 267 nm. Measuring the THG spectrum at 267 nm is problematic because the spectral response of the silicon detector arrays in most spectrometers changes rapidly across wavelengths in that region of the UV. Alternatively, one can generate the difference frequency (DFG) between the SHG and fundamental pulses. This cascaded $\chi^{(2)}$ process would produce a pulse at the fundamental wavelength. This is experimentally more complicated as it involves spatially and temporally overlapping the SHG and fundamental beams in a crystal. Also, because the intensity of the fundamental beam will be much higher than that of the DFG, the mixing of the SHG and fundamental must be noncollinear so that the DFG comes out at a different angle than the other two beams. Even though the fundamental and DFG beams will be orthogonally polarized, the extinction ratio of a polarizer will not be great enough to fully separate the two. It is hoped that with more algorithm development and optimization taken with experimental validation with a Ti:sapphire laser system that SPINS will fill a niche that no other technique has been able to fill: single-shot pulse retrieval from beams with poor-quality wavefronts.

References

- [1] Rick Trebino. Autocorrelation tutorial. http://swamptoptics.com/tutorials_autocorrelation.htm.
- [2] Rick Trebino. *Frequency-Resolved Optical Gating: The Measurement of Ultrashort Laser Pulses*. Kluwer Academic Publishers Group, Norwell, MA, USA, 2000.
- [3] R.N. Bracewell. *The Fourier Transform and Its Applications, 2nd Ed.* McGraw-Hill, New York, NY, USA, 1986.
- [4] Jean-Claude Diels and Wolfgang Rudolph. *Ultrashort Laser Pulse Phenomena*. Academic Press, San Diego, CA, USA, 1996.
- [5] Rick Trebino. Interferometric autocorrelation tutorial. http://swamptoptics.com/tutorials_interferometric.htm.
- [6] Kazunori Naganuma, Kazuo Mogi, and Hajime Yamada. General method for ultrashort light pulse chirp measurement. *IEEE J. Quantum Electronics*, 25(6):1225–1233, jun 1989.
- [7] J.W. Nicholson, J. Jasapara, W. Rudolph, F.G. Omenetto, and A.J. Taylor. Full-field characterization of femtosecond pulses by spectrum and cross-correlation measurements. *Optics Letters*, 24(23):1774–1776, dec 1999.
- [8] Toshiyuki Hirayama and Mansoor Sheik-Bahae. Real-time chirp diagnostic for ultrashort laser pulses. *Optics Letters*, 27(10):860–862, may 2002.
- [9] Daniel Bender and Mansoor Sheik-Bahae. Modified spectrum autointerferometric correlation (mosaic) for single-shot pulse characterization. *Optics Letters*, 32(19):2822–2824, oct 2007.
- [10] Y. Ishida, K. Naganuma, and T. Yajima. Self-phase modulation in hybridly mode-locked cw dye lasers. *IEEE J. Quantum Electronics*, 10(1):69–77, jan 1985.

References

- [11] Rick Trebino. Frog tutorial. http://swampoptics.com/tutorials_FROG.htm.
- [12] Chris Iaconis and Ian A. Walmsley. Self-referencing spectral interferometry for measuring ultrashort optical pulses. *IEEE J. Quantum Electronics*, 35(4):501–509, apr 1999.
- [13] Rick Trebino. Spider tutorial. http://swampoptics.com/tutorials_spider.htm.
- [14] Ian Walmsley. Spider algorithm. <http://ultrafast.physics.ox.ac.uk/spider/inversion.pdf>.